Solid Freeform Fabrication 2023: Proceedings of the 34th Annual International
Solid Freeform Fabrication Symposium – An Additive Manufacturing Conference
Reviewed Paper

MULTIPLE 450 nm DIODE LASER PROCESSING OF TI64 POWDER

H.Caglar*, A. Liang*, K. Mumtaz*

*Department of Mechanical Engineering, The University of Sheffield, Sheffield, S1 4BJ, United Kingdom

Abstract

Diode Area Melting (DAM) presents an alternative approach to traditional Laser Powder Bed Fusion (PBF-LB/M) approaches, integrating multiple individually addressable low-power fibre-coupled diode lasers into a laser head; these traverse across a powder bed to melt powdered feedstock. DAM research to date has focused on using low-power 808 nm lasers to process Ti-6Al-4V (Ti64) powder. This work focuses on using multiple short wavelengths 450 nm 4W lasers to process Ti64 feedstock. Previous studies found that when processing Ti64, absorption was 11% higher using 450 nm lasers when compared to using 808 nm lasers and 14% higher than 1064nm laser. This work demonstrated the potential to use shorter wavelength lasers in DAM/LPBF for improved melting efficiency. Also, it aimed to examine the impact of 450 nm diode lasers on Ti64 and generate a parameter map for this material. It was found that low power (4W) multiple 450 nm diode lasers can successfully melt the Ti64 for AM applications with above 95% density.

1. Introduction

PBF-LB is used worldwide in the metal additive manufacturing (AM) sector. Laser PBF is used in aerospace, automotive, and various sectors requiring near-net shape processes, low waste material output during the manufacturing stage, high customisation, and almost impossible to produce with traditional subtractive manufacturing systems. However, the current PBF-LB systems require high laser power output, and the scalability is poor due to nature of the size of the laser components [2], [3]. To overcome these challenges, a new system was developed which can accommodate multiple short-wavelength diode lasers (3-5W per laser) to melt the metal powder to achieve dense parts as SLM can do while increasing the processing window of the powder bed. The integrated multiple lasers with arrays are scanning the layer at transverse orientation (Figure 1 – (a)). As it scans the area and melts it simultaneously, the name of the technology is known as Diode Area Melting (DAM) [2-5].

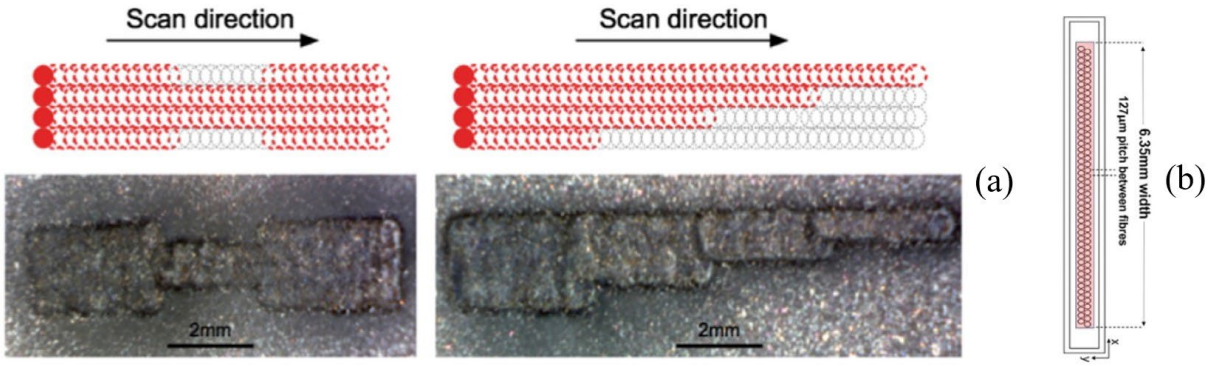

Figure 1 - (a) Illustration of a sample with single pass [2], (b) Example of a bottom view of multiple fibres of lasers in arrays [5]

PBF-LB primarily utilises high-quality alloys like Inconel, aluminium, and titanium alloys [1], [2]. Aerospace, energy, automotive, and medical industries frequently prefer titanium alloys due to their exceptional strength-to-weight ratio, corrosion resistance, wear resistance, fracture toughness, fatigue resistance, and excellent weldability in laser AM. [6].

1.1. Comparison of Area Melting with Diodes and current SLM systems

The key theoretical benefits of DAM were explained in previous studies [1-5], such as faster build speed, smaller laser unit size, low cost, high compatibility of multimode laser orientation, high resolution with small, focused lasers in arrays, independent high speed for the size of the geometry, greater electrical to optical output, greater melting efficiency.

The spot size of a laser beam focused on a powder bed is crucial for achieving desired part quality and accuracy. A smaller spot size results in higher energy density, improving resolution and feature details. However, it also increases the number of laser passes required and can prolong manufacturing time. The DAM system can process geometry with fewer passes compared to the SLM system due to its large spot size. [1], DAM is [80-175 μm per laser] x [number of lasers] [2],[5],[4]) while not compromising the quality of small spot size SLM parts. The lasers were generally orientated in arrays (Figure 1-(b)). The desired shape or passes could be defined within the dimensions of the spot size. Oppositely, a larger spot size covers a larger area in each pass, reducing the overall processing time. Yet, it may result in reduced resolution and lower precision due to a wider heat-affected zone and potential energy spill over to adjacent powder particles.

The absorptivity of the laser radiation by the metallic powders plays a crucial role in the efficiency and quality of the powder-bed fusion process. Laser absorptivity refers to the ability of a material to absorb laser energy and convert it into heat. In the context of metallic powders, absorptivity depends on various factors such as powder composition, particle size, morphology, and surface roughness. A higher absorptivity allows for more efficient energy absorption, leading to faster and more complete powder melting. Additionally, it promotes better fusion between the individual powder particles, resulting in improved structural integrity and mechanical properties of the final manufactured component. Conversely, a lower absorptivity may lead to insufficient energy absorption, incomplete melting, and weakened bonding between the powder particles. The previous studies showed that when a laser's wavelength decreases, the energy's absorption rate increases on metal powder. Ehlers et al. [1], [7] conducted an investigation revealing that the absorptivity of aluminium can be enhanced by approximately 13% when employing an 808 nm high-power diode laser instead of utilising 1064 nm fibre lasers. Similarly, Alsaddah et al. [1], [2] conducted studies on Ti64 and discovered that the absorption rate was 11% higher when employing 450 nm lasers in comparison to 808 nm lasers and 14% higher when compared to 1064-nm lasers. Furthermore, Alsaddah et al. affirmed that employing an 808 nm diode laser in the DAM process enables the production of high-density parts exceeding 95% density. [1], [5]. The authors indicated that this phenomenon primarily arises from the shorter wavelength characteristic of the lasers used, resulting in reduced reflectivity of the powder compared to 1064 nm lasers. Consequently, the relatively lower power lasers could effectively melt the Ti64 powder, overcoming reflectivity challenges.

The cooling rate may be delineated as the temporal interval during which laser energy is administered to induce the liquefaction of metallic powders. Subsequently, the ensuing cooling

process exerts a discernible impact on the solidification dynamics and resultant microstructural characteristics. Consequently, the duration of time elapsed within these conditions may be called the cooling rate. LPBF systems cooling rates can go up to 10^7°K/s while DAM can process slow as 800°K/s while using 1064-1070 nm and 808 nm, respectively [5]. A higher cooling rate promotes rapid solidification, producing finer grain structures and enhanced mechanical properties such as improved strength and hardness. At the same time, it increases the residual stress, which affects the dimensional accuracy and the cosmetic appearance of the sample (such as warping, distortion, and cracking). Conversely, a slower cooling rate allows for more time for the material to rearrange and form larger grain structures. It also helps reduce the formation of undesirable defects, such as porosity and segregation. Therefore, controlling the cooling rate during powder-bed fusion is essential for achieving the desired microstructure, optimising the mechanical performance, and controlling the residual stress of the manufactured components.

The DAM methodology replaces the traditional galvo scanning methodology within a single fibre laser SLM system with multiple non-deflected low-power laser diode beams that scan and selectively melt powdered feedstock material in parallel. The ability to process materials with melt temperatures above 1400°C using DAM has been demonstrated by Zavala-Arredondo et al. [3]. A multilayer stainless-steel sample with cross-sectional micro-density areas comparable to SLM has been reported. In addition, it has been found that there are fewer studies about 450 nm (blue) diode laser sources related to powder-bed fusion. A few studies investigated that blue laser can melt metal powders and create high-density parts [1], [8–10].

Moreover, Alsaddah et al. [1] scrutinised that blue laser can melt Ti64 powders as dense as the 808 nm diode laser. However, that study was done under the single laser mode. There is a noticeable absence of research addressing the parameters and their impact on materials when it comes to multiple 450 nm diode lasers. This study will investigate the parametric study of the processing of Ti64 with multiple 450 nm diode lasers, laser-powder interaction, densification, and surface roughness data compared with the literature.

2. Experimental Methodology

2.1. DAM's laser processing technology

The DAM process integrates collimating and focusing lenses to achieve localised melting within the designated area. The assemblage of these lenses, in conjunction with a multi-laser head holder, is called the Computer-to-Plate (CtP) Head. A schematic depiction showcasing the operational workflow of a CtP head is illustrated in Figure 2, elucidating the key stages involved in the process with DAM. After this stage, the remaining steps in the Diode Area Melting (DAM) process mirror those employed in conventional LPBF systems. There are powder-bed pistons and a gantry system for CtP Head in a closed chamber. As the levels of the powder-bed decrease (can be set in between 10-1000 μm), the reservoir progressively rises. Then, a wiper blade is deployed to distribute the powder uniformly, forming a fresh layer.

Afterwards, the CtP head processes the layer. These steps signify a commonality between DAM and traditional SLM systems, ensuring consistency in the overall process flow. For this study, a stainless steel 316L substrate was utilised. The substrate had holes, allowing for the sample

removal procedure without causing any damage. The laser beam passed over the targeted area during the process, causing the molten material to seep into the holes. Upon solidification, this material served as an anchorage for the subsequent layers to be built upon. Implementing this particular substrate configuration resulted in significant enhancements in surface wettability, improved adherence to the substrate, and minimal thermal deformation (warpage) when compared to a flat substrate. The processing window is 40x40 mm^2. The layer was spread with a silicone-based wiper to enhance the uniformity of the layer. Argon was purged into the chamber to reduce oxidisation and fire risk. The experimental procedure was never started when the O_2 content was higher than 0.09%. The argon circulation was done via an air blade which becomes operational when the O_2 content is low enough.

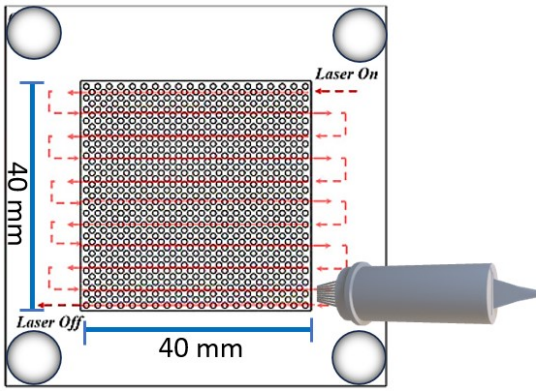

Figure 2 - SS316L Substrate with the diagram of the scanning strategy

The scanning strategy for this study was limited to one-way zigzag, as shown in Figure 2. CtP Head was never tilted or rotated during the scanning was happening. The operational speed limit for the CtP gantry system is 10-1000 mm/min. Laser operating temperatures were monitored during this investigation. During the setup, lasers were tested at different temperatures, scanning the powder bed without temperature control.

It was found that the operating temperature window had a huge impact on the optical power output. The optical power output was reduced significantly (from 4W to 2.5W) when the laser's temperature were below 10°C. Then, the operating temperature for lasers was set between 15-20°C and the issue were fixed permanently. DAM consisted of 4 separate systems. In order to start the process, the powder pistons controller (ΔZ) needs to be used to arrange first and rest of the layers, then the CtP gantry controller (ΔX-Y) needs to be engaged to move the CtP to the start/end position of the layer. After that, lasers can be turned on/off (ΔP) after checking the temperature (ΔT) of the laser modules is in between 15-20°C to start (Figure 3). Those movements had been done manually for each layer in this study.

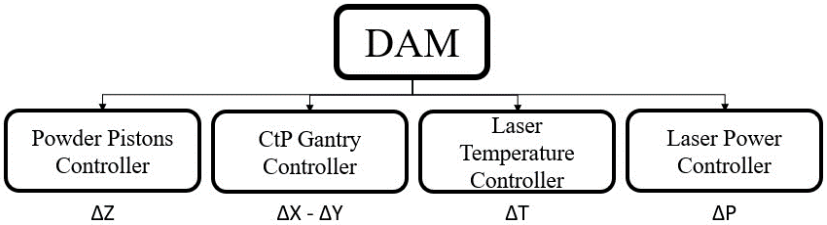

Figure 3 - Operational Procedure Diagram of DAM

2.2. Material Specifications

This research uses gas-atomised Ti6Al4V Grade 23 LPBF (flexible) feedstock from Carpenter Additive. This material can also be found as Ti. Gr.23, CL 41 TI ELI, Ti64ELI, Ti6Al4V ELI-0406 [6]. Particle size distribution is 15-45 µm (90%) and it has been stated by the manufacturer as spherical. The other specifications are mentioned in Table 1.

Table 1 - Ti6Al4V Grade23 specifications

Chemical Composition									
Element	Ti	Al	V	Fe	O	C	N	H	Y
wt%	Balance	5.5-6.5	3.5-4.5	0.25	0.13	0.08	0.03	0.0125	0.005

Physical Properties at 1604°C			**units**
Specific Heat Capacity	(C_p)	0.5263	J/g.°C
Melting Temperature	(T_m)	1604	°C
Material Density	(d)	4430	Kg/m^3
Thermal Diffusivity	(D)	$6.7x10^{-6}$	m^2/s
Absorptivity at 450nm	(A)	72	%

2.3. Laser Specifications and Beam Characterisation Process

In this study, a new CtP head was deployed to a bespoke DAM system to make the system compatible with 450 nm studies. The new CtP head accommodates 50 laser fibres into one array, each located 127 µm apart. The designated focal length of the CtP head is 60 mm. The laser specifications are given in Table 2, used in this study. Nine lasers were integrated into the CtP head for this study, as the Peltier cooling module was capable of cooling down a maximum of nine lasers at the same time. The beam shape and size of the lasers were measured with NanoScan2sPryo/9/5 (Table 2). During the profilometer scanning, the laser power was set to 0.7A (around 1W per laser (±0.1)). In Figure 4 – (e), the spot size seems to be non-uniform elliptical because the nine lasers were just under the focused spot capturing slot as it was around 700 µm.

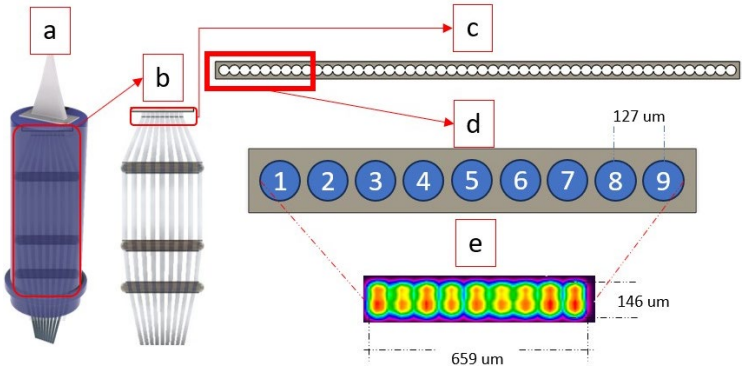

Table 2 - Laser Specifications

Laser specifications per each laser		
Maximum Power	4.2	W
Wavelength	450±10	nm
50% Width	52 x 72	µm
9-laser specifications		
Maximum Power	36	W
50% Width	659x146	µm

Figure 4 - (a) CtP Head, (b) laser head, collimating and focusing lenses, (c) focused bottom view of laser head, (d) 9 active laser fibre orientation in this study, (e) beam profile that of 9 lasers

The power was not changed during the experiments as during the setup procedure, and it was found that below 3W of power was not adequate to melt any of the samples with Ti64 powder. The laser manufacturer did not recommend the increments to be lower than 0.5W. Therefore, the experiments were conducted with 4W optical focused output per laser as 3.5W 450 nm was studied [1]. In total, the power output calculated for the area is approximately 36W.

2.4. Design of Experiments

Firstly, single-track studies were conducted in Table 3-(1) to create a parameter map for optimum region for Ti64 on 450 nm DAM, and after investigation, parameters were narrowed down to Table 3-(2). Then with the optimum two of the track parameters, the hatch distance (HD) study was performed as a single layer (3). Afterwards, optimum layer thickness studies were done within the selected high dense HD parameters (4). These studies and the parameters are mentioned in Table 3 below. All parameters were deposited/printed three times to prove repeatability. Where P is for "Power", SS is "Scanning Speed", HD is for "Hatch Distance", LH is for "Layer Height", SSHD is coding to represent the parameters (i.e. SS50HD800LH200 means 50mm/min speed, 800 µm hatch spacing, 200 µm layer thickness) as well as SSHDLH.

Table 3 - Parameter region used in this study

Expanded Single Track Parameters (1)				**Narrowed Single Track Parameters (2)**			
P	36	W		P	36	W	
SS	50, 100-1000	mm/min	100 inc.	SS	20-90	mm/min	10 inc.
Size	20	mm		Size	20	mm	
Hatch Distance Parameters (3)				**Layer Thickness Parameters (4)**			
P	36	W		P	36	W	
SS	50, 75	mm/min		SSHD	50-800, 75-700	mm/min- µm	
HD	400-1200	µm	100 inc.	LH	400,200,100	µm	
Size	5x5	mm^2		#L	20 (5x5mm)	Layers	

Density measurement was calculated from a cross sectional view for the multilayers after the material preparation procedure. This procedure involved hot mounting, cutting half to see the build direction view, grinding from 320 grit to 2500 grit, and polishing with 0.06 µm colloidal silica solution. The average surface roughness was measured using an optical 3D microscope (Alicona infinite focus) with 5 different line patterns (R_a) at 5x zoom. A scanning electron microscope (SEM) (Tescan VEGA3) and a Nikon optical microscope were used to create images. Images were processed using ImageJ, and values were averaged after three attempted measurements.

2.5. Normalised Energy Density

According to Alsaddah et al. [1] scrutinised the normalised energy density adaptation on DAM. Therefore, it can be said that the region of $4.5<E^*<14.8$ claimed to achieve high-density parts (>95%). Furthermore, it can be said that the region of $4.5<E^*<8$ produces above >99% dense

parts when gathering the information from the previous studies [1], [5]. The normalised energy equation for DAM was defined as;

$$E^* = \frac{P^*}{v^* l^*} = \frac{AP}{2vlr\rho C_\rho (T_m - T_0)} \quad (1)[5]$$

$$r = (n * 2r_b) + ((n-1) * d_g) \quad (2)[5]$$

Where A is the material absorption at the wavelength of lasers used in the current work (450 nm), ρ is the material density (kg·m^3), $C\rho$ is the specific heat (J·kg^{-1}·k^{-1}), v is the scanning speed (m·s^{-1}), T_0 ambient temperature (K), T_m powder bed temperature (K) and r beam radius (m). the length of the beam replaces r as this study investigates/uses a rectangular beam rather than a Gaussian shape. Where n is the number of lasers, r_b is the radius of a laser, and d_g is the separation distance between each laser.

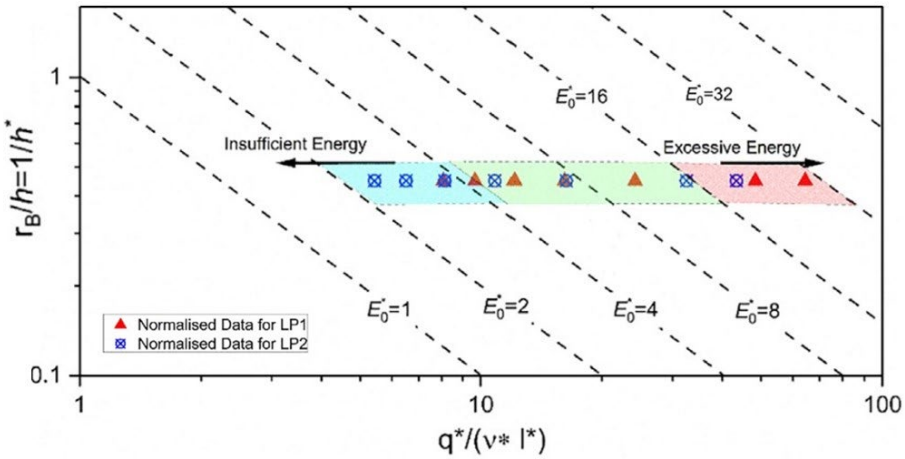

Figure 5 – Parameter Map with Normalised Energy Density (NED) chart from Alsaddah et al. [5] study

According to Alsaddah et al. [5], Figure 5 presented illustrates a normalised processing diagram depicting normalised energy density "E^*" shown on the x-axis and normalised hatch "h^*" on the y-axis using a log10 scale. The isopleth dashed lines indicate the minimum energy input "E_0" required to melt the material at a specific volume "$2rl^*$". The green area, ranging from 4.5 to 14.8, represents the normalised processing parameters resulting in high-density parts with a density greater than 95%. Conversely, using processing parameters resulting in an energy density within the red zone defined by E_0>14.8 leads to excessive energy, causing material vaporisation. A lack of fusion occurs when employing processing parameters that provide "E_0" less than 4.5 (i.e. within the blue region). In this particular scenario, it is apparent that the energy supplied is inadequate to achieve the melting of the powder layers, resulting in a density reduction below the threshold of 90%.

3. Results and Discussion

3.1. Effects of the number of lasers on powder-bed

First, the correlation between the number of diode lasers on a melt pool width was studied to understand the size difference of melt pool dimensions with sequential active lasers. The powder

was spread onto a 1000 µm thick layer. The scanning speed was 50 mm/min. The speed value was selected based on a previous study [1]. The sample size was set to 20 mm as they were single tracks. Five measurements were taken from different locations of the SEM pictures (Figure 7). The influence of the spot size on the melt pool width showed that the number of active laser spot size is larger than 75% in terms of melt pool width. A linear equation was derived from Figure 6 to forecast the melt pool size with the number of lasers to put an accurate HD value while fabrication of multilayer ($R^2 \approx 1$). To calculate melt pool width, an equation is generalised from the data. Moreover, when the number of lasers increases, the melt pool depth and width also increase.

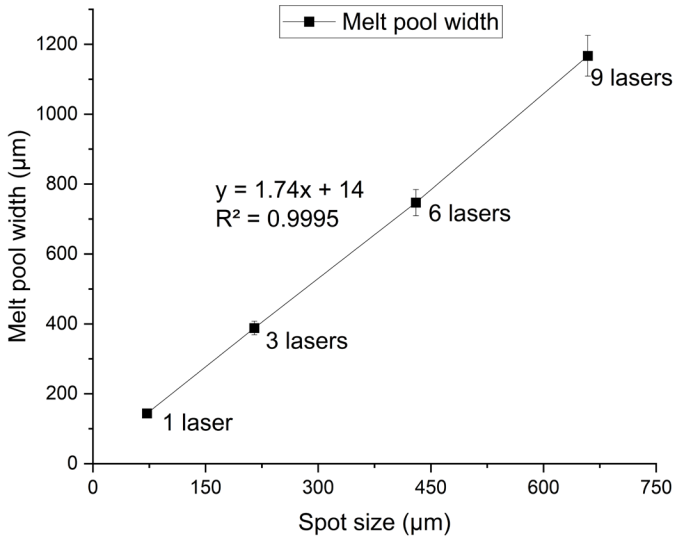

Figure 6 - Correlation between melt pool width and active sequential laser spot size on powder-bed

$$M_W = 1.74\ (n * d_{laser}) + 14 \quad (3)$$

Where M_W is melt pool width, n is the number of activated lasers in sequential, d_{laser} is the 50% Width of a single beam (X-axis). The number of active lasers can also be represented as the total optical power output since it delivers power to a specific area. The aim here is to comprehend the correlation between the depth and width of the melt pool and the total power output. As illustrated in Figure 8 (left), when the laser power increases, both the depth and width exhibit an increase. However, it is worth noting that the trend in the increment of melt pool depth appears to be slowing down. Therefore, it can be inferred that when the laser head is operating at its maximum laser output capacity, there may exist a consistent melt pool width that remains unaffected by the power output.

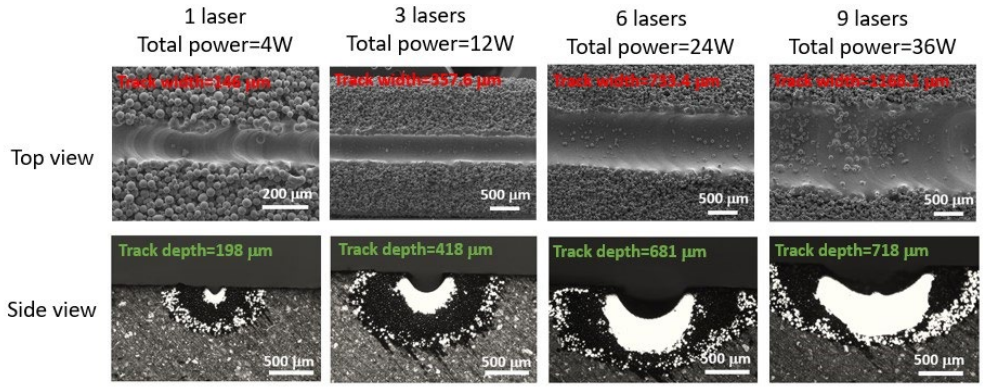

Figure 7 - Top and side view of samples used in melt pool-spot size chart

On the other hand, a dataset from Table 3 – Section 1 and Section 2 was used to create single tracks on a 1000 µm thick layer. Figure 8 [right] shows a focused parameter study with nine lasers (36W) reflecting on melt pool width and depth. First, there is an upward trend from 20 mm/min to 80 mm/min for melt pool width, but this trend continues towards 100 mm/min for melt pool depth. This phenomenon can be elucidated by considering the heat dissipation mechanisms within the powders. Heat transfer dynamics exhibit distinct characteristics when powder is employed as a substrate, as is the case here. Nonetheless, these observed trends provide a preliminary insight into the rate and manner in which optimal heat transfer levels are attained. Furthermore, they tend to expand in dimensions between 300 mm/min and 500 mm/min. The dimensions of the samples increased in height and depth due to balling phenomena. Yet, once the speed reached 500 mm/min, both dimensions decreased, and defects emerged.

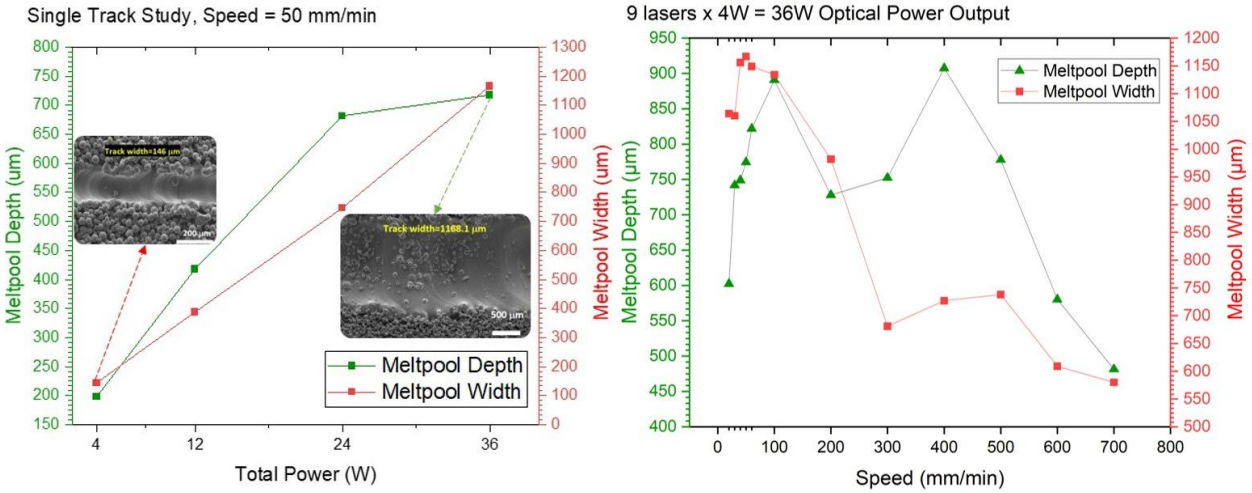

Figure 8 - [Left] Correlation between melt pool depth (green) and melt pool width (red) with total power corresponding to active lasers, [Right] Correlation between melt pool depth (green) and melt pool width (red) with a speed of CtP Head. All data points are an average.

Following the measurement of the melt pool depth, the layer height was subsequently reduced to 500 µm to assess the wetting characteristics. During the single-track study, several observations were made by assessing the physical appearances of the samples which those are heat affected zone (HAZ) around the sample, cracks, spattering effect, balling phenomenon, wetting capabilities to the substrate, and track continuity. To quantify spattering, an observer employed a

chronometer, while wetting behaviour was determined by observing whether the sample adhered to the substrate or not during removal. A comprehensive list of these defects and observations is presented in Table 4. It is evident that the HAZ exhibits a notable discrepancy concerning scan speed. An intriguing discovery pertains to spattering. When the scan speed is constrained to as low as 20 or 50 mm/min, owing to the inherent nature of the DAM system, spattering is nearly absent or occurs at an exceedingly low rate, with fewer than five particles per second. This is markedly lower in comparison to current LPBF systems.

Table 4 - Single Track Observation/Defect Chart with 9 Lasers

Parameters	**Observations / Defects**					
Speed (mm/min)	HAZ (µm)	Cracks	Spatter (particles/s)	Balling	Wetting	Continuity
20	≈2000	Major	0-2	No	Adequate	Yes
30	≈1000	Minor	0-3	No	Adequate	Yes
40	≈500	No	1-3	No	Adequate	Yes
50	≈450	No	1-4	No	Adequate	Yes
60	≈400	No	2-5	No	Adequate	Yes
70	≈300	No	2-5	No	Adequate	Yes
80-200	300 - 200	No	10-30	Yes	Moderate	Yes
300-500	≈200	No	30+	Yes	Not Enough	Yes
600-1000	≈200-500	N/A	High (50+)	Yes	Not Enough	No

3.2. Hatch distance (overlap) studies

The hatch distance (HD) studies, or in other words, overlap studies, were done using the dataset of Table 3 – (3). The importance of this investigation was to obtain the optimum overlap value for the maximum density possible while not compromising the surface roughness quality. Two outcomes were considered: top surface density and top surface roughness. According to Table 5, it was found that the optimum region was selected between 600 µm and 800 µm as they showed the highest surface densities without compromising the surface roughness for the layer after which will be spread (green). The importance of R_a is that if the higher region is more than the layer thickness, the wiper will hit the sample's highest point, potentially destroying the sample (red). The surface density for the low HD values (HD400 and HD500) is higher than 99% for both samples while getting the smallest average R_a values. However, due to high energy input, solidification cracks were observed partially. Consequently, it makes them in risky parameters region (yellow).

Table 5 - Parameters used in Hatch Distance (HD) study

Speed	50 mm/min and 75 mm/min (18 parameters in total)								
HD (µm)	400	500	600	700	800	900	1000	1100	1200
Overlap (%)	64.4	55.5	46.6	37.7	28.8	19.9	11.0	2.1	-6.8
	Low Ra but minor cracks		Top surface density > 99%			Top surface density < 90% High Ra			

The roughness data (Figure 9) were collected from a single layer of HD study samples to understand the influence of normalised energy density (NED) on the top surface roughness. LH was assumed to be 100 µm in NED calculations to make the calculations comparable with multilayer studies (Figure 9). When the NED increases, the R_a generally shows a downward trend, especially if NED is higher than 15, R_a can be lower than 10, which is smoother than some SLM-processed parts [11].

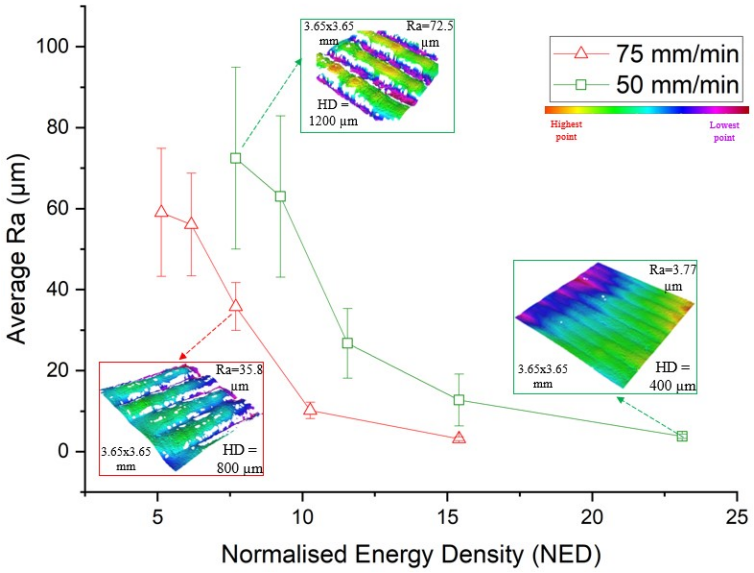

NED	HD (µm)	SS (mm/min)
23.1	400	50
15.4	600	50
11.6	800	50
9.2	1000	50
7.7	1200	50
15.4	400	75
10.3	600	75
7.7	800	75
6.2	1000	75
5.1	1200	75

Figure 9 - Correlation between Average Ra of the top surface of a sample and Normalised Energy Density (NED)

3.3. Optimising the layer height for multilayer studies

The data in Figure 8 shows that melt pool depth can be as profound as 942 µm. According to this data set, a layer height investigation was conducted. The range started from 800 µm and lowered to 100 µm by lowering half each time. The outputs are mentioned in Table 6.

Table 6 - Parameters used in Layer Height (LH) study and observations

SS (mm/min)	HD (µm)	LH (µm)	Density (%)	Observations
50	800	800	N/A	Delamination due to not enough wetting
50	800	400	75.0	High sintering between layers, not enough wetting
50	800	200	87.4	Moderate sintering between layers
50	600	100	96.2	More than half of the layers were connected
75	700	800	N/A	Delamination due to not enough wetting
75	700	400	69.5	High sintering between layers, not enough wetting
75	700	200	85.8	Moderate sintering between layers
75	600	100	95.4	Less connection compared to 50 mm/min

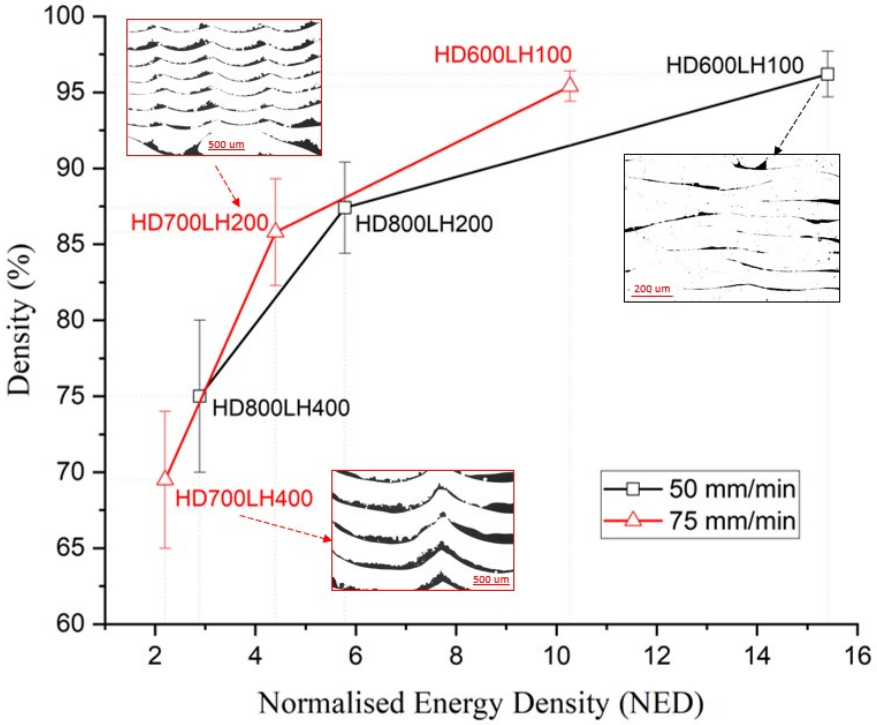

Figure 10 - Correlation between density in build direction and Normalised Energy Density (NED)

As shown in Figure 10, whenever the NED increases, the density increases as well. As was expected, the study gives similar results to Alsaddah et al. [5] work. However, this study found that the region between $7.7<E_0<15.4$ gives excellent results for the multilayer Ti64. The reason can be based on the wavelength, the absorptivity based on this material, and the spot size/power ratio, as they are the key attributes in this NED calculation. Moreover, higher NED samples need to be investigated as it needs to show when this trend starts to go downwards so that the maximum point can be found, and this energy can be used to increase speed which has the most detrimental effect on time. To prove that the theoretical calculations were made. These calculations show the required time to process a layer (5x5 mm^2) and a cube (5x5x5 mm^3). In Figure 11, it is evident that the relative change in SS is more pronounced than that of HD, suggesting a potentially greater influence. Nevertheless, it is important to note that when both parameters exhibit the same relative change, the impact on the system remains consistent.

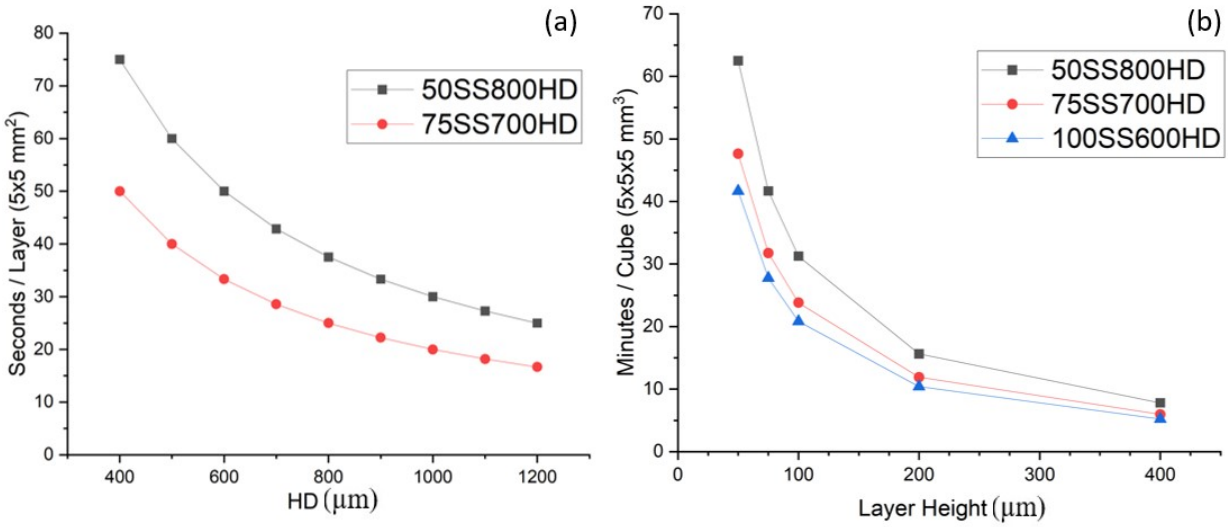

Figure 11 - (a) Time required to process 5x5 mm² sample, (b) Time required to process 5x5x5 mm³ sample. SS is mm/min, and HD is in µm

4. Conclusions

This investigation has demonstrated the potential of a multiple 450 nm diode laser (4W each) on the DAM approach utilising fibre optics as a promising and scalable alternative to conventional LPBF techniques. By leveraging this methodology, large scale spot size (>600 µm) was created with the transverse laser beam profiles. The study primarily focused on developing a parameter map for Grade 23 Ti64 using 450 nm multiple diode lasers in DAM. The obtained results substantiate the successful melting of Ti64 using this system. Furthermore, the investigation examined the influence of multiple beam profiles on the melt pool, revealing that the width and depth of the melt pool increase with the number of lasers employed. Additionally, the study investigated the effects of speed, hatch distance, and layer thicknesses, highlighting the crucial role of normalised energy density (NED). The parameter map was established based on NED, and the samples exhibited exceptional bonding characteristics without any discernible defects when the NED value ranged between 7.7-15.4. In addition, the study identified that employing 20 layers with a layer thickness of 100 µm and other optimised parameters could achieve a density exceeding 95%. It was observed that the top surface porosity increased with hatch distance. To gain further insights, the study recommends investigating additional parameters based on the reciprocal of the NED (1/h*) axis, as it would establish limits considering material chemistry, the required time for continuous solidification, and the minimum duration necessary to prevent vaporisation of elements. Furthermore, the study emphasises the need for microstructural and mechanical investigations to ensure consistent and reliable outcomes for Grade 23 Ti64.

REFERENCES

[1] M. Alsaddah, A. Khan, K. Groom, and K. Mumtaz, “Use of 450-808 nm diode lasers for efficient energy absorption during powder bed fusion of Ti6Al4V,” *Int. J. Adv. Manuf. Technol.*, vol. 113, no. 9–10, pp. 2461–2480, Apr. 2021, doi: 10.1007/s00170-021-06774-4.

[2] M. Zavala-Arredondo *et al.*, “Laser diode area melting for high speed additive manufacturing of metallic components,” *Mater. Des.*, vol. 117, pp. 305–315, Mar. 2017, doi: 10.1016/j.matdes.2016.12.095.
[3] M. Zavala-Arredondo, K. M. Groom, and K. Mumtaz, “Diode area melting single-layer parametric analysis of 316L stainless steel powder,” *Int. J. Adv. Manuf. Technol.*, vol. 94, no. 5–8, pp. 2563–2576, 2018, doi: 10.1007/s00170-017-1040-4.
[4] M. Zavala-Arredondo, H. Ali, K. M. Groom, and K. Mumtaz, “Investigating the melt pool properties and thermal effects of multi-laser diode area melting,” *Int. J. Adv. Manuf. Technol.*, vol. 97, no. 1–4, pp. 1383–1396, 2018, doi: 10.1007/s00170-018-2038-2.
[5] M. Alsaddah, A. Khan, K. Groom, and K. Mumtaz, “Diode area melting of Ti6Al4V using 808 nm laser sources and variable multi-beam profiles,” *Mater. Des.*, vol. 215, p. 110518, Mar. 2022, doi: 10.1016/j.matdes.2022.110518.
[6] Carpenter Additive, “PowderRange Ti64 datasheet,” pp. 1–7, 2020, [Online]. Available: https://www.carpenteradditive.com/powderrange-powders.
[7] B. Ehlers, H.-J. Herfurth, and S. Heinemann, “Hardening and welding with high-power diode lasers,” *Laser Diodes LEDs Ind. Meas. Imaging, Sensors Appl. II; Testing, Packag. Reliab. Semicond. Lasers V*, vol. 3945, no. March 2000, p. 63, 2000, doi: 10.1117/12.380556.
[8] K. Ono, Y. Sato, R. Higashino, Y. Funada, N. Abe, and M. Tsukamoto, “Pure copper rod formation by multibeam laser metal deposition method with blue diode lasers,” *J. Laser Appl.*, vol. 33, no. 1, p. 012013, Feb. 2021, doi: 10.2351/7.0000322.
[9] S. Masuno *et al.*, “Metal powder bed fusion additive manufacturing with 100W blue diode laser,” p. P130, Dec. 2019, doi: 10.2351/1.5138180.
[10] R. Higashino *et al.*, “Development of blue diode laser for additive manufacturing,” in *Laser 3D Manufacturing VII*, Mar. 2020, vol. 32, no. 7, p. 41, doi: 10.1117/12.2543119.
[11] K. Mumtaz and N. Hopkinson, “Top surface and side roughness of Inconel 625 parts processed using selective laser melting,” *Rapid Prototyp. J.*, vol. 15, no. 2, pp. 96–103, Mar. 2009, doi: 10.1108/13552540910943397.